Proton acceleration from high-contrast short pulse lasers interacting with sub-micron thin foils

G. M. Petrov, C. McGuffey, A. G. R. Thomas, K. Krushelnick, and F. N. Beg

---

Articles you may be interested in

Generation of a quasi-monoenergetic high energy proton beam from a vacuum-sandwiched double layer target irradiated by an ultraintense laser pulse
Phys. Plasmas **21**, 043110 (2014); 10.1063/1.4871862

Recent progress in particle acceleration from the interaction between thin-foil targets and J-KAREN laser pulses
AIP Conf. Proc. **1465**, 133 (2012); 10.1063/1.4737552

A compact post-acceleration scheme for laser-generated protons
Phys. Plasmas **18**, 073103 (2011); 10.1063/1.3574361

Influence of a preplasma on electron heating and proton acceleration in ultraintense laser-foil interaction
J. Appl. Phys. **104**, 103307 (2008); 10.1063/1.3028274

Particle selection for laser-accelerated proton therapy feasibility study
Med. Phys. **30**, 1660 (2003); 10.1118/1.1586268

Proton acceleration from high-contrast short pulse lasers interacting with sub-micron thin foils

G. M. Petrov,[1,a)] C. McGuffey,[2] A. G. R. Thomas,[3] K. Krushelnick,[3] and F. N. Beg[2]

[1]*Naval Research Laboratory, Plasma Physics Division, 4555 Overlook Ave. SW, Washington, DC 20375, USA*
[2]*Mechanical and Aerospace Engineering and Center for Energy Research, University of California-San Diego, La Jolla, California 92093, USA*
[3]*Center for Ultrafast Optical Science, University of Michigan, Ann Arbor, Michigan 48109, USA*

A theoretical study complemented with published experimental data of proton acceleration from sub-micron (thickness $< 1\,\mu m$) foils irradiated by ultra-high contrast ($>10^{10}$) short pulse lasers is presented. The underlying physics issues pertinent to proton acceleration are addressed using two-dimensional particle-in-cell simulations. For laser energy $\varepsilon \leq 4\,J$ (intensity $I \leq 5 \times 10^{20}\,\mathrm{W/cm^2}$), simulation predictions agree with experimental data, both exhibiting scaling superior to Target Normal Sheath Acceleration's model. Anomalous behavior was observed for $\varepsilon > 4\,J$ ($I > 5 \times 10^{20}\,\mathrm{W/cm^2}$), for which the measured maximum proton energies were much lower than predicted by scaling and these simulations. This unexpected behavior could not be explained within the frame of the model, and we conjecture that pre-pulses preceding the main pulse by picoseconds may be responsible. If technological issues can be resolved, energetic proton beams could be generated for a wide range of applications such as nuclear physics, radiography, and medical science.
© 2016 AIP Publishing LLC. [http://dx.doi.org/10.1063/1.4941318]

I. INTRODUCTION

Short pulse lasers at sufficiently high intensities can function as compact particle accelerators. Ion beams with particle kinetic energy in the tens and hundreds of MeV can be generated from thin (0.01–$10\,\mu m$) foils irradiated by short pulse lasers with intensity 10^{19}–$10^{22}\,\mathrm{W/cm^2}$ and duration 30–700 fs. Many applications can benefit from proton beams with improved quality. Examples include fast ignition physics,[1] laser nuclear physics,[2] neutron production,[3] proton radiography,[4] and cancer therapy.[5] There is an extensive body of research on proton generation in the Target Normal Sheath Acceleration (TNSA) regime. High laser intensity and short timescale dynamics are believed to be the path to produce proton beams with superior scaling. In addition, major advancement is expected to come from the utilization of ultrathin ($\ll 1\,\mu m$) foils, which can harness the potential of novel acceleration mechanisms to produce monoenergetic beams. The successful implementation of these ideas may lead to widespread applications, which is strong incentive to continue investigating the production of proton beams.

Owing to the Chirped Pulse Amplification technique, the laser intensity can now reach unprecedented levels, on the order of $10^{22}\,\mathrm{W/cm^2}$. More recent advances in laser technology made progress in another direction: cleaning up the pulse thus reducing the pico- and nanosecond pre-pulse levels below the damage threshold of the material. Contemporary laser systems equipped with dual plasma mirrors (DPM) have contrast levels as high as 10^{15},[6] which allows the utilization of ultrathin ($\ll 1\,\mu m$) foils as laser targets. The combination of high laser intensities, high contrast, and ultrathin targets made possible the exploration of new exotic regimes of particle acceleration.

Depending on foil thickness and to some extent laser pulse duration, the ion acceleration mechanisms fall into three general categories:[7] Coulomb explosion,[8] volumetric acceleration, and TNSA.[9] In the case of the first category, if the foil is too thin ($<10\,nm$), the laser field can completely remove all electrons in the central laser spot and the ions left behind Coulomb explode on their own. In the opposite extreme of thick foils ($>200\,nm$), only a thin layer of ions on the back surface of the foil is accelerated. This is essentially *surface* acceleration, also characterized by poor coupling of laser energy to ions. Both regimes have been thoroughly investigated and the ion acceleration mechanisms are well known. In the intermediate regime ($10 < L < 200\,nm$), when the foil thickness is comparable to the relativistic skin depth, the laser field can reach all the way to the back of the foil (hole-boring) and the *whole volume* of the plasma in front of the laser is pushed forward, maximizing the energy absorption.[7] This is better known as relativistic transparency regime, which is rich in physics and is by far the most challenging for exploration and interpretation. For example, numerous acceleration mechanisms such as radiation pressure acceleration (RPA),[10–12] breakout afterburner,[13] laser-piston,[14] and shock acceleration[15] have been identified. We refrain from discussing specific ion acceleration mechanisms; instead, we provide an up-to-date collection of experimental data and comparison to particle-in-cell (PIC) simulations.

The present study is a natural extension of previous work on proton acceleration. It is motivated by their significance for both fundamental research and applications. The goals set forth include: (i) assemble and analyze

experimental data on proton acceleration from ultrathin foils (20–500 nm), (ii) compare measured maximum proton energies to simulation results, and (iii) develop scaling laws for proton acceleration from ultrathin foils in the high-contrast regime. In Section II, we review available experimental data on maximum proton energy and construct appropriate scaling versus foil thickness, laser intensity, and energy. The monotonous increase of maximum proton energy versus laser intensity and energy unexpectedly halts, which prompted to consider the impact of picosecond pre-pulses, as discussed in Section III. A summary of the paper is presented in Section IV.

II. MAXIMUM PROTON ENERGY SCALING

A. Maximum proton energy versus foil thickness

Available experimental data[6,16–32] for proton acceleration from sub-micron foils are listed in Table I. What these laser systems have in common is the large nanosecond pre-pulse contrast (10^{10} and better), allowing interaction with sub-micron foils. The foil thickness plays a crucial role in the process of proton acceleration. Foils that are either too thin (a few nm) or too thick (a few microns) do not couple laser energy efficiently. Best coupling is achieved when the foil thickness is between the two extremes. A rough estimate for the optimum foil thickness L^{opt} assuming that it extends a few relativistic skin depths,[7] $\ell_{skin} = \gamma^{1/2} c/\omega_p$, yields $L^{opt} \cong 20 - 100$ nm. The parameters $\gamma = \sqrt{1 + a_0^2}$ and $\omega_p = \sqrt{n_e e_0^2/(\varepsilon_0 m_e)}$ are the relativistic parameter and electron plasma frequency, respectively; $a_0 = e_0 E_0/(m_e \omega_0 c)$ is the normalized laser field amplitude; E_0 and ω_0 are the amplitude and frequency of the laser field; e_0, n_e, and m_e are the electron charge, number density, and mass; ε_0 is the permittivity of free space; and c is the speed of light. The energy coupling also depends on other factors such as pre-plasma generated by nanosecond and picosecond pre-pulses.

According to the experimental data listed in Table I, the maximum proton energy was found to decrease with foil thickness increasing.[6,16–22] These findings are consistent with 2D PIC simulations[33] shown in Figure 1. Specifically, we used the Hercules laser parameters (peak intensity $I_0 = 2.75 \times 10^{20}$ W/cm^2, pulse duration $\tau_{FWHM} = 40$ fs, spot size $D_{FWHM} = 4.5\ \mu m$, wavelength $\lambda_0 = 0.8\ \mu m$, and energy $\varepsilon = 2.5$ J) to investigate foil thickness effect. The target is a 98 μm wide flat Si$_3$N$_4$ foil (density 3.2 g/cm^3) with various thicknesses (10–1000 nm), having a 5 nm H$_2$O contamination layer on the back. The simulation box is a square with dimensions $100 \times 100\ \mu m^2$, the cell size is 20×20 nm^2, and the time step is $\Delta t = 0.01 \lambda_0/c$.
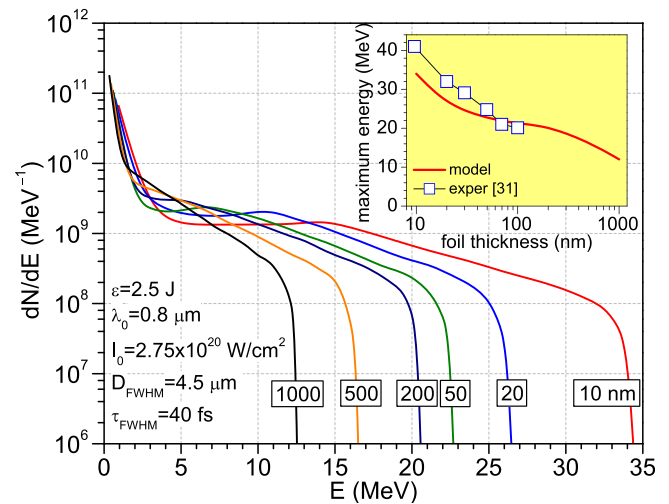

FIG. 1. PIC calculated proton spectra from Si$_3$N$_4$ foil for thicknesses between 10 nm and 1 μm. Laser parameters: $I_0 = 2.75 \times 10^{20}$ W/cm^2, $\tau_{FWHM} = 40$ fs, $D_{FWHM} = 4.5\ \mu m$, $\lambda_0 = 0.8\ \mu m$, and $\varepsilon = 2.5$ J. Inset: calculated maximum proton energy versus foil thicknesses (solid line) and data from the experiment with the closest laser parameters: intensity 3×10^{20} W/cm^2 and pulse duration 30 fs (open symbols).[31]

TABLE I. Maximum proton energy from ultrathin foils measured at various laser facilities. Laser parameters: peak intensity, duration (FWHM), spot size (FWHM), energy on target as reported by authors, laser fluence, and laser wavelength. Foil parameters: material and thickness. The laser fluence, calculated according to $F = I_0 \tau_{FWHM}$ may not match the one calculated from laser energy and spot size, $F = 4\varepsilon/(\pi D_{FWHM}^2)$.

Laser facility	I$_0$ (W/cm^2)	τ (fs)	D (μm)	E (J)	F (J/μm^2)	λ (μm)	Foil	L (nm)	E$_{max}$ (MeV)	Ref.
Trident	7×10^{19}	700	10	40	4.9×10^{-1}	1.05	DLC	50	25	24
Trident	2×10^{20}	500	9.4	90	1.0×10^{0}	1.05	DLC	42	37	26
LULI	1×10^{18}	320	18	1	3.2×10^{-3}	1.06	SiN	30	7.3	29,30
Saclay	5×10^{18}	65	8	0.2	3.3×10^{-3}	0.8	Mylar	80	5	19,20
Astra-Gemini	7×10^{20}	50	2.5	5.8	3.0×10^{-1}	0.8	Al	100	8.2	18
Astra-Gemini	7×10^{20}	50	2.5	5.8	3.0×10^{-1}	0.8	C	100	7.5	18
Astra-Gemini	2×10^{20}	50	2.5	6	1.0×10^{-1}	0.8	Al	50	12	16
Max Born Institute	5×10^{19}	45	3.6	0.7	2.3×10^{-2}	0.8	DLC	5–50	8	25
Max Born Institute	5×10^{19}	45	3.6	0.7	2.3×10^{-2}	0.8	DLC	5	12	27
Max Born Institute	2×10^{19}	40	6	0.2	8.0×10^{-3}	0.8	SiN	30	3.5	23
Hercules	2×10^{21}	40	1.2	1.3	8.0×10^{-1}	0.8	SiN	30–500	12	6
Hercules	2×10^{21}	40	1.2	1.1	8.0×10^{-1}	0.8	CH$_2$	100	20	32
Lund	1×10^{19}	33	10	0.3	3.3×10^{-3}	0.8	Al	30	3.5	22
Scarlet	5×10^{20}	30	5	4	1.5×10^{-1}	0.8	SiN	100	10	28
Pulser I	3×10^{20}	30	5.8	8	1.0×10^{-1}	0.8	F8BT	10	45	31
ALLS	1×10^{20}	30	5.6	1.8	3.0×10^{-2}	0.8	Al	120	10	17
Salle Jaune	4×10^{19}	30	5	0.25	1.2×10^{-2}	0.8	Al	400	3.7	21

B. Maximum proton energy versus laser intensity

In Figure 2, the maximum proton energy is plotted versus peak laser intensity spanning from 10^{18} W/cm^2 to 2×10^{21} W/cm^2. The data are separated into two groups: "ultra-short" (30–65 fs) and "short" (500–700 fs) laser pulses. The rationale behind these two classifications for pulse lengths is that the first group contains a large number of laser systems, mostly at universities around the globe, while the second group contains laser systems that are limited in numbers but have significantly higher laser energies. More importantly, the pulse duration of the two groups differ by one order of magnitude, which entails different acceleration mechanisms (for example, RPA for the first group,[10–12] BoA for the second[13,14]). For this reason, two sets of simulation results are presented, one for "ultra-short" (40 fs) and one for "short" (400 fs) pulses, using a 50 nm Si$_3$N$_4$ foil. Experimental data come from a variety of foil materials (see Table I), and in order to study the impact of the material, we performed an additional set of simulations with a 50 nm diamond-like carbon foil (density 2.7 g/cm^3). The calculated maximum proton energies were comparable to those of Si$_3$N$_4$ and the trends were akin. The experimental data from "short" laser pulses fall into two distinct categories. The first one follows the expected trend and increases with laser intensity. However, at $I \cong 3 \times 10^{20}$ W/cm^2, this trend abruptly changes. The maximum proton energies measured in three separate experiments did not exceed $\sim$12 MeV. Such behavior was completely unexpected. In contrast, the simulations show a clear trend of increasing the maximum proton energy with laser intensity and no saturation.

Much work has been devoted to the maximum proton energy scaling for thick foils ($>1\,\mu$m) in the TNSA regime.[34–36] Though it depends on the particular laser and foil conditions, it is typically between $E_{max} \sim I^{1/3}$[34] and $E_{max} \sim I^{1/2}$.[36] Our simulations show that for sub-micron foils the maximum proton energy scales as $\sim I^{2/3}$ (short pulse) and $\sim I^{4/5}$ (long pulse),

both stronger than TNSA. The different scaling laws for thick ($>1\,\mu$m) and ultrathin ($\ll 1\,\mu$m) foils can be explained qualitatively by noting that for TNSA, the laser cannot interact directly with the protons on the back of the foil and fast electrons originating from the front side must go through the foil and form a space-charge sheath on the back surface in order to mediate the proton acceleration, while for ultrathin foils the laser field interacts *directly* with the proton layer on the back surface of the foil. The direct interaction, sometimes called enhanced TNSA, naturally leads to higher power dependence.

C. Maximum proton energy versus laser energy

The short pulse experimental data have been obtained for laser pulses operating at different conditions, specifically, laser intensity and spot size. To assess the impact of the latter, additional simulations were performed varying the spot size from 1.5 to 10 μm. It was established that for $D_{FWHM} < 5 - 6\,\mu$m, E_{max} scales linearly with D_{FWHM}, and only for $D_{FWHM} > 6\,\mu$m, the maximum proton energy is independent of the focal spot size (Figure 3, inset). Due to the strong dependence of E_{max} on both the intensity and focal spot size, it would be more appropriate to compare the data plotted in Figure 2 as a function of laser energy.[37] Except for three points, the short pulse data agree well with the simulations. Moreover, they follow a power dependence of the form $E_{max} \sim \varepsilon^{3/5}$, identical to that predicted by the PIC simulations. But for laser energy on target $\varepsilon \geq 4\,J$, roughly corresponding to power $P \geq 100$ TW, there is a set of "anomalous" data that do not follow this scaling.[16,18,28] In all three experiments, the measured maximum proton energy remains limited to only $\sim$12 MeV. We conjecture that in these experiments, pre-pulses on picosecond-to-nanosecond timescale may be the limiting factor. This issue will be discussed next in detail.

III. THE IMPACT OF PRE-PULSES ON MAXIMUM PROTON ENERGY

The most likely explanation for the drop of maximum proton energy at large laser energy is that the thinnest foils
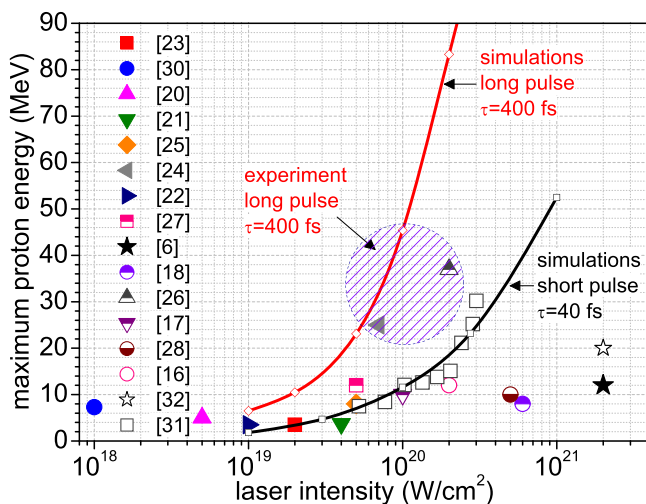

FIG. 2. Maximum proton energy versus laser intensity. Symbols: experimental data with varied laser parameters and target thickness, open squares are for 30 nm foil.[31] Lines: simulations for a 50 nm Si$_3$N$_4$ foil with 5 nm H$_2$O contaminants. Back solid line $\tau_{FWHM} = 40$ fs, $D_{FWHM} = 4.5\,\mu$m, red solid line: $\tau_{FWHM} = 400$ fs, $D_{FWHM} = 4.5\,\mu$m. The shaded area contains the experimental data for long pulse.
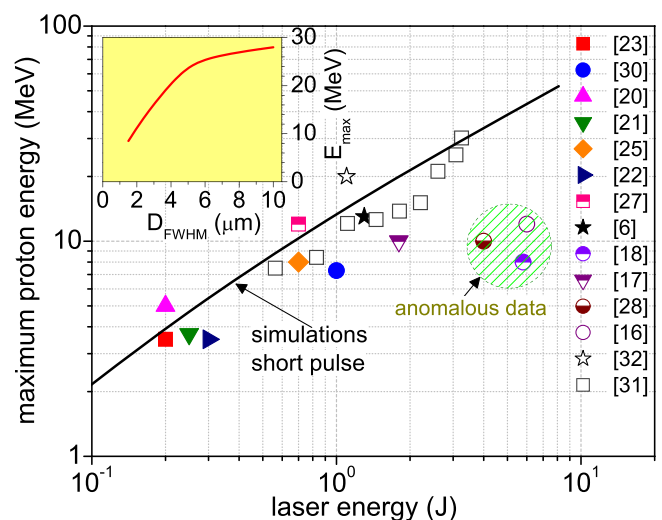

FIG. 3. Maximum proton energy versus laser energy. The shaded area contains the anomalous data region. Inset: calculated maximum proton energy versus focal spot size.

(<100 nm) are susceptible to low-intensity picosecond pre-pulses having fluence comparable to the damage threshold of the material. The pre-pulse conditions for the "anomalous" data are, indeed, close to or slightly exceed the material damage threshold (Table II). The pre-pulse launches a high velocity (a few km/s) shock wave which propagates through the target.[38] For thick targets and/or low pedestal intensities, the shock is weak and attenuates inside. The foil is mildly disturbed and remains flat (scenario #1). For thin targets and/or high pre-pulse intensities, the shock can break out on the rear side before the arrival of the main pulse causing severe foil deformation, e.g., bending it in an ark[38,39] (scenario #2). The two cases are schematically illustrated in Figure 4. Simultaneously, the whole foil, whose thickness is just one-two skin depths,[40] including the contaminant layer, is heated to temperature of several eV causing ablation of the proton layer. A 5 nm layer moving with the sound speed, which is on the order of $(2-3) \times 10^6$ cm/s, would expand to $\sim$500 nm for the duration of the pre-pulse ($\sim$20 ps (Refs. 16 and 18)). The main pulse will interact with low density proton/oxygen plasma spread over a large volume. For thick targets and/or low pedestal intensities (scenario #1), the expansion length ($\sim$0.5 μm) is much smaller than the transverse dimension (4–5 μm focal spot size) and the expansion is close to one-dimensional. In the opposite case, the expansion is multi-dimensional. The outcome for the two scenarios is demonstrated by PIC simulations. One-dimensional expansion of the proton layer (scenario #1) yields a proton spectrum in the forward direction, which is very close to that from an unperturbed layer (Figure 5). Expansion in 2D from a deformed target (scenario #2) yields lower maximum proton energies and smaller number of energetic protons. This is the most likely outcome for the targets listed in Table II.

TABLE II. Target parameters, pre-pulse parameters, and damage threshold fluence for metal and dielectrics.[39] The reported pre-pulse contrast is 10^{10}.

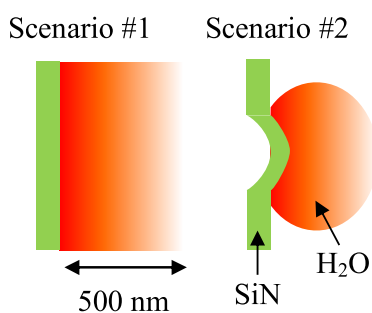| Laser facility	Target	I_{ASE} (W/cm^2)	τ_{ASE} (ps)	F_{ASE} (J/cm^2)	F_{thr} (J/cm^2)	Ref.
Astra-Gemini	100 nm Al	7×10^{10}	20	1.4	0.4	18
Astra-Gemini	100 nm C	7×10^{10}	20	1.4	6.0	18
Astra-Gemini	50 nm Al	2×10^{10}	20	0.4	0.4	16
Scarlet	100 nm SiN	5×10^{10}	10^3	50	40	28

FIG. 4. A schematics of weakly perturbed foil for thick targets and/or low pedestal intensities (scenario #1) and target deformation for thin targets and/or high pedestal intensities (scenario #2). The contaminants blow-off in 1D (left) and 2D (right) are shown in receding gradient red.
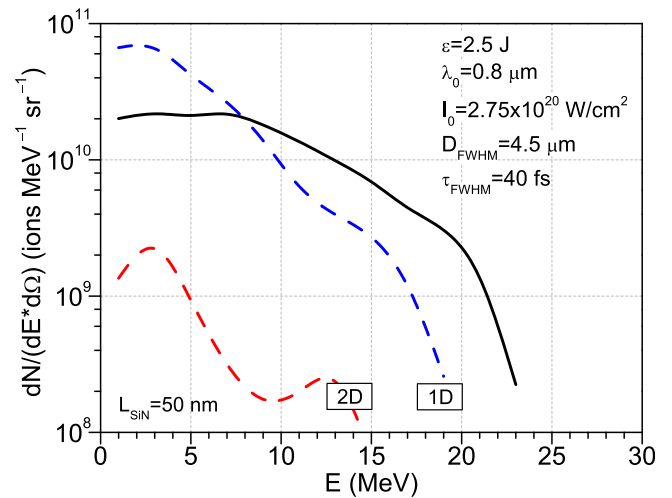

FIG. 5. Calculated proton spectra $\frac{d^2N}{dEd\Omega}$ in the forward direction from a 50 nm Si$_3$N$_4$ foil having an intact 5 nm contaminant layer at liquid density (black solid line) and 500 nm expanded contaminants layer densities (dashed lines) in 1D (scenario #1) and 2D (scenario #2). Blue dashed line: 1D expansion model. The density is equal to 1/100 the original density, and the number of protons/oxygen ions is equal to that in the pre-expanded layer. Red dashed line: 2D expansion model. The density and number are reduced by a factor of $1/10^4$ and 1/100, respectively. The laser parameters are the same as in Figure 1.

Shock wave with velocity $\sim$5 km/s (5 nm/ps) will reach the rear of the foil by the end of the pre-pulse, causing target deformation (Figure 4, right). The reduced number of energetic protons is particularly detrimental for detection, since the proton number may drop below the detection level. For the experimental conditions of Ref. 16, a Thompson parabola with opening angle 9×10^{-9} sr will collect only a few energetic protons.

A similar scenario was previously investigated on the Hercules laser.[6] Two cases were examined, one where only the inherent laser pulse cleaning capabilities were used (XPW) and the pre-pulse pedestal level was above the damage threshold, and another in which DPM configuration was used reducing the pre-pulse level below the damage threshold ((Ref. 6), Figure 2). The clean (below damage threshold) DPM pulses interacting with 30–50 nm SiN foils produced much higher maximum proton energies ($\sim$10 MeV) compared to the low-contrast XPW case, which produced only 2 MeV protons ((Ref. 6), Figure 4). Numerical simulations performed for both cases also showed lower maximum proton energies from deformed targets compared to targets that remain intact.

IV. SUMMARY AND CONCLUSIONS

Published experimental data on maximum proton energy from ultrathin foils generated by short pulse lasers in the high-contrast regime have been compared to 2D PIC simulations. The experimental data agree with the simulations up to laser energy on target 4 J (intensity 3×10^{20} W/cm^2). Beyond this energy/intensity, the measured maximum proton energies are lower than predicted and saturate at $\sim$12 MeV. By comparing pre-pulse conditions to material damage threshold, we conjecture that picosecond pre-pulses

inherently present in laser systems may be responsible. Therefore, the effect of picosecond pre-pulses on ultrathin targets needs to be critically evaluated. It should be noted, however, that in the above-mentioned experiments, the pre-pulse conditions were actually not far from what may be considered as "clean pre-pulse" and minor improvements can dramatically improve the beam energy. At least in one case, the pre-pulse technical issues at laser intensities around $\sim 10^{21}$ W/cm² have been resolved[31] and the proton beam properties follow the expected trend. With laser technology constantly advancing and progress made in improving pre-pulse conditions, ultra-thin targets and ultra-high contrast lasers promise compact high repetition rate energetic particle sources for applications such as nuclear physics, radiography, and medical science.

ACKNOWLEDGMENTS

[1]M. Roth, T. E. Cowan, M. H. Key, S. P. Hatchett, C. Brown, W. Fountain, J. Johnson, D. M. Pennington, R. A. Snavely, S. C. Wilks, K. Yasuike, H. Ruhl, F. Pegoraro, S. V. Bulanov, E. M. Campbell, M. D. Perry, and H. Powell, Phys. Rev. Lett. **86**, 436 (2001).

[2]P. McKenna, K. W. D. Ledingham, T. McCanny, R. P. Singhal, I. Spencer, M. I. K. Santala, F. N. Beg, K. Krushelnick, M. Tatarakis, M. S. Wei, E. L. Clark, R. J. Clarke, K. L. Lancaster, P. A. Norreys, K. Spohr, R. Chapman, and M. Zepf, Phys. Rev. Lett. **91**, 075006 (2003).

[3]D. P. Higginson, J. M. McNaney, D. C. Swift, G. M. Petrov, J. Davis, J. A. Frenje, L. C. Jarrott, R. Kodama, K. L. Lancaster, A. J. Mackinnon, H. Nakamura, P. K. Patel, G. Tynan, and F. N. Beg, Phys. Plasmas **18**, 100703 (2011).

[4]M. Borghesi, A. Schiavi, D. H. Campbell, M. G. Haines, O. Willi, A. J. Mackinnon, P. Patel, M. Galimberti, and L. A. Gizzi, Rev. Sci. Instrum. **74**, 1688 (2003).

[5]M. Goitein, A. J. Lomax, and E. S. Pedroni, Phys. Today **55**(9), 45 (2002).

[6]F. Dollar, C. Zulick, T. Matsuoka, C. McGuffey, S. S. Bulanov, V. Chvykov, J. Davis, G. Kalinchenko, G. M. Petrov, L. Willingale, V. Yanovsky, A. Maksimchuk, A. G. R. Thomas, and K. Krushelnick, Phys. Plasmas **20**, 056703 (2013).

[7]G. M. Petrov and J. Davis, Appl. Phys. B **96**, 773 (2009).

[8]S. S. Bulanov, A. Brantov, V. Yu. Bychenkov, V. Chvykov, G. Kalinchenko, T. Matsuoka, P. Rousseau, S. Reed, V. Yanovsky, K. Krushelnick, D. W. Litzenberg, and A. Maksimchuk, Med. Phys. **35**, 1770 (2008).

[9]S. C. Wilks, A. B. Langdon, T. E. Cowan, M. Roth, M. Singh, S. Hatchett, M. H. Key, D. Pennington, A. MacKinnon, and R. A. Snavely, Phys. Plasmas **8**, 542 (2001).

[10]S. C. Wilks, W. L. Kruer, M. Tabak, and A. B. Langton, Phys. Rev. Lett. **69**, 1383 (1992).

[11]B. Qiao, M. Zepf, M. Borghesi, and M. Geissler, Phys. Rev. Lett. **102**, 145002 (2009).

[12]A. Macci, S. Veghini, and F. Pegoraro, Phys. Rev. Lett. **103**, 085003 (2009).

[13]L. Yin, B. J. Albright, B. M. Hegelich, K. J. Bowers, K. A. Flippo, T. J. T. Kwan, and J. C. Fernandez, Phys. Plasmas **14**, 056706 (2007).

[14]T. Esirkepov, M. Borghesi, S. V. Bulanov, G. Mourou, and T. Tajima, Phys. Rev. Lett. **92**, 175003 (2004).

[15]L. O. Silva, M. Marti, J. R. Davies, R. A. Fonseca, C. Ren, F. S. Tsung, and W. B. Mori, Phys. Rev. Lett. **92**, 015002 (2004).

[16]R. Prasad, A. A. Andreev, S. Ter-Avetisyan, D. Doria, K. E. Quinn, L. Romagnani, C. M. Brenner, D. C. Carroll, N. P. Dover, D. Neely, P. S. Foster, P. Gallegos, J. S. Green, P. McKenna, Z. Najmudin, C. A. J. Palmer, J. Schreiber, M. J. V. Streeter, O. Tresca, M. Zepf, and M. Borghesi, Appl. Phys. Lett. **99**, 121504 (2011).

[17]S. Fourmaux, S. Buffechoux, B. Albertazzi, D. Capelli, A. Lévy, S. Gnedyuk, L. Lecherbourg, P. Lassonde, S. Payeur, P. Antici, H. Pepin, R. S. Marjoribanks, J. Fuchs, and J. C. Kieffer, Phys. Plasmas **20**, 013110 (2013).

[18]D. C. Carroll, O. Tresca, R. Prasad, L. Romagnani, P. S. Foster, P. Gallegos, S. Ter-Avetisyan, J. S. Green, M. J. V. Streeter, N. Dover, C. A. J. Palmer, C. M. Brenner, F. H. Cameron, K. E. Quinn, J. Schreiber, A. P. L. Robinson, T. Baeva, M. N. Quinn, X. H. Yuan, Z. Najmudin, M. Zepf, D. Neely, M. Borghesi, and P. McKenna, New J. Phys. **12**, 045020 (2010).

[19]T. Ceccotti, A. Levy, H. Popescu, F. Reau, P. D'Oliveira, P. Monot, J. P. Geindre, E. Lefebvre, and Ph. Martin, Phys. Rev. Lett. **99**, 185002 (2007).

[20]T. Ceccotti, A. Levy, F. Reau, H. Popescu, P. Monot, E. Lefebvre, and Ph. Martin, Plasma Phys. Controlled Fusion **50**, 124006 (2008).

[21]A. Flacco, F. Sylla, M. Veltcheva, M. Carrié, R. Nuter, E. Lefebvre, D. Batani, and V. Malka, Phys. Rev. E **81**, 036405 (2010).

[22]D. Neely, P. Foster, A. Robinson, F. Lindau, O. Lundh, A. Persson, C.-G. Wahlström, and P. McKenna, Appl. Phys. Lett. **89**, 021502 (2006).

[23]A. A. Andreev, S. Steinke, T. Sokollik, M. Schnürer, S. Ter Avetsiyan, K. Yu. Platonov, and P. V. Nickles, Phys. Plasmas **16**, 013103 (2009).

[24]A. Henig, D. Kiefer, K. Markey, D. C. Gautier, K. A. Flippo, S. Letzring, R. P. Johnson, T. Shimada, L. Yin, B. J. Albright, K. J. Bowers, J. C. Fernandez, S. G. Rykovanov, H.-C. Wu, M. Zepf, D. Jung, V. Kh. Liechtenstein, J. Schreiber, D. Habs, and B. M. Hegelich, Phys. Rev. Lett. **103**, 045002 (2009).

[25]A. Henig, S. Steinke, M. Schünrer, T. Sokollik, R. Hörlein, D. Kiefer, D. Jung, J. Schreiber, B. M. Hegelich, X. Q. Yan, J. Meyer-ter-Vehn, T. Tajima, P. V. Nickles, W. Sandner, and D. Habs, Phys. Rev. Lett. **103**, 245003 (2009).

[26]D. Kiefer, A. Henig, D. Jung, D. C. Gautier, K. A. Flippo, S. A. Gaillard, S. Letzring, R. P. Johnson, R. C. Shah, T. Shimada, J. C. Fernandez, V. Kh. Liechtenstein, J. Schreiber, B. M. Hegelich, and D. Habs, Eur. Phys. J. D **55**, 427 (2009).

[27]S. Steinke, M. Schnürer, T. Sokollik, A. A. Andreev, P. V. Nickles, A. Henig, R. Hörlein, D. Kiefer, D. Jung, J. Schreiber, T. Tajima, M. Hegelich, D. Habs, and W. Sandner, Contrib. Plasma Phys. **51**, 444 (2011).

[28]P. L. Poole, C. D. Andereck, D. W. Schumacher, R. L. Daskalova, S. Feister, K. M. George, C. Willis, K. U. Akli, and E. A. Chowdhury, Phys. Plasmas **21**, 063109 (2014).

[29]P. Antici, J. Fuchs, E. d'Humières, E. Lefebvre, M. Borghesi, E. Brambrink, C. A. Cecchetti, S. Gaillard, L. Romagnani, Y. Sentoku, T. Toncian, O. Willi, P. Audebert, and H. Pépin, Phys. Plasmas **14**, 030701 (2007).

[30]P. Antici, J. Fuchs, E. d'Humières, E. Lefebvre, M. Borghesi, E. Brambrink, C. A. Cecchetti, S. Gaillard, L. Romagnani, Y. Sentoku, T. Toncian, P. Audebert, and H. Pépin, IEEE Trans. Plasma Sci. **36**, 1817 (2008).

[31]I. J. Kim, K. H. Pae, C. M. Kim, H. T. Kim, J. H. Sung, S. K. Lee, T. J. Yu, I. W. Choi, C.-L. Lee, K. H. Nam, P. V. Nickles, T. M. Jeong, and J. Lee, Phys. Rev. Lett. **111**, 165003 (2013).

[32]F. Dollar, S. A. Reed, T. Matsuoka, S. S. Bulanov, V. Chvykov, G. Kalintchenko, C. McGuffey, P. Rousseau, A. G. R. Thomas, L. Willingale, V. Yanovsky, D. W. Litzenberg, K. Krushelnick, and A. Maksimchuk, Appl. Phys. Lett. **103**, 141117 (2013).

[33]G. M. Petrov and J. Davis, Phys. Plasmas **18**, 073102 (2011).

[34]F. N. Beg, A. R. Bell, A. E. Dangor, C. N. Danson, A. P. Fews, M. E. Glinsky, B. A. Hammel, P. Lee, P. A. Norreys, and M. Tatarakis, Phys. Plasmas **4**, 447 (1997).

[35]J. Fuchs, P. Antici, E. D'Humieres, E. Lefebvre, M. Borghesi, E. Brambrink, C. A. Cecchetti, M. Kaluza, V. Malka, M. Manclossi, S. Meyroneinc, P. Mora, J. Schreiber, T. Toncian, H. Pepin, and P. Audebert, Nat. Phys. **2**, 48 (2006).

[36]K. Krushelnick, E. L. Clark, F. N. Beg, A. E. Dangor, Z. Najmudin, P. A. Norreys, M. Wei, and M. Zepf, Plasma Phys. Controlled Fusion **47**, B451 (2005).

[37]J. Schreiber, F. Bell, and Z. Najmudin, High Power Laser Sci. Eng. **2**, e41 (2014).

[38]O. Lundh, F. Lindau, A. Persson, C.-G. Wahlström, P. McKenna, and D. Batani, Phys. Rev. E **76**, 026404 (2007).

[39]D. Batani, Laser Part. Beams **28**, 235 (2010).

[40]E. G. Gamaly, A. V. Rode, B. Luther-Davies, and V. T. Tikhonchuk, Phys. Plasmas **9**, 949 (2002).